Behavioral/Systems/Cognitive

Ipsilateral Hand Input to Area 3b Revealed by Converging Hemodynamic and Electrophysiological Analyses in Macaque Monkeys

Michael L. Lipton,* Kai-Ming G. Fu,* Craig A. Branch, and Charles E. Schroeder

Center for Advanced Brain Imaging and Cognitive Neuroscience Program, The Nathan S. Kline Institute for Psychiatric Research, Orangeburg, New York 10962, and Departments of Radiology and Neuroscience, Albert Einstein College of Medicine and Montefiore Medical Center, Bronx, New York 10467

Functional magnetic resonance imaging (fMRI) of the hand representation in primary somatosensory cortex (area 3b) of macaque monkeys revealed an ipsilateral hand input undetected by most previous studies. Ipsilateral responses had a hemodynamic signature indistinguishable from that of contralateral hand responses. We explored the neural mechanisms of the fMRI effects using a second derivative analysis of field potentials [current source density (CSD) analysis] combined with action potential profiles, sampled from area 3b using linear array multielectrodes. In contrast to the predominantly excitatory contralateral response, the colocated ipsilateral response appeared dominated by inhibition, suggesting that ipsilateral inputs may have modulatory effects on contralateral input processing. Our findings confirm bimanual convergence at the earliest stage of cortical somatosensory processing in primates. They also illustrate the value of combined CSD and fMRI analyses in monkeys for defining hidden aspects of sensory function and for investigating the neuronal processes generating fMRI signals.

Key words: **somatosensory physiology; ipsilateral response; fMRI; monkey area 3b; cortical feedback; inhibition**

Introduction

In primates, combination of tactile information from the two hands to form a bilateral representation provides a substrate for efficient processing and integration of somatosensory inputs during bimanual tasks (Iwamura et al., 1994; Iwamura, 1998). Bilateral and ipsilateral hand representations are found in S2 (Whitsel et al., 1969), area 5 (Sakata et al., 1973), and even in area 2 (Iwamura et al., 1994). In area 3b, the overt hand representation thus far appears to be exclusively contralateral, despite the fact that it can be modulated by stimulation of the ipsilateral hand (Calford and Tweedale, 1990). In this regard, the hand representation in primate area 3b contrasts strongly with that in carnivores (Towe et al., 1964) and rodents (Shin et al., 1997), as well as with the primary cortical representations of the face, oral cavity (Dreyer et al., 1975; Manger et al., 1996; Jain et al., 2001; Disbrow et al., 2003), and midline trunk (Conti et al., 1986) that commonly incorporate and/or cross the midline. These physiological findings mirror known anatomical constraints, because the hand representation in area 3b appears to lack direct thalamic inputs driven by the ipsilateral hand and has few callosal connections (Jones and Hendry, 1980; Killackey et al., 1983).

Paradoxically, preliminary findings from functional magnetic resonance imaging (fMRI) experiments in anesthetized macaques demonstrated a robust hemodynamic response in the hand region of area 3b during stimulation of the ipsilateral median nerve (Lipton et al., 2003). To define the underlying neuronal activity, we probed the fMRI findings by also using direct neural measurements.

Because the blood-oxygen-level-dependent (BOLD) fMRI signal appears more closely associated with local field potentials (LFPs) than action potentials (Lauritzen and Gold, 2003; Logothetis, 2003), we examined LFP distributions. However, we took the extra steps of applying current source density (CSD) analysis (Freeman and Stone, 1969; Nicholson and Freeman, 1975) to the LFPs and of measuring concomitant multiunit activity (MUA). CSD analysis defines the laminar transmembrane current flow profile underlying LFPs, localizing activity within specific cortical layers and neuron populations, and MUA helps to distinguish net excitatory and inhibitory processes (Schroeder et al., 1998).

Materials and Methods

fMRI

Subjects. Three *Macaca mulatta* were imaged.

Stimuli. Mechanical stimulation used a custom pneumatically driven device, brushing the palm and fingers at 1 Hz. Electrical stimulation of the median nerve at the wrist used two subcutaneous gold needle electrodes inserted 1 cm apart overlying the nerve. Electrical stimulation from a GRASS S8 stimulator (Grass Instruments, Quincy, MA) delivered a 200 μs duration square wave pulse at 1 Hz. Stimulus intensity was

Received March 18, 2005; revised Oct. 28, 2005; accepted Oct. 29, 2005.

This work was supported in part by National Institutes of Health Grants K08-MH67082-01 (M.L.L.) and RO1-MH44794 (C.E.S., C.A.B., M.L.L.). We acknowledge the technical assistance of Noelle O'Connell, Scott Gerum, and Tammy McGuiness and the histological analysis performed by Dr. John Smiley. We also thank Dr. Robert Desimone for comments on a previous version of this manuscript.

*M.L.L. and K.-M.G.F. contributed equally to this work.

Correspondence should be addressed to Dr. Charles E. Schroeder, The Nathan S. Kline Institute for Psychiatric Research, 140 Old Orangeburg Road, Orangeburg, NY 10962. E-mail: schrod@nki.rfmh,org.

DOI:10.1523/JNEUROSCI.1073-05.2006

 0270-6474/06/260180-06$15.00/0

titrated before each session to just subthreshold for the adductor pollicis brevis twitch. Stimulation was assessed after each session to ensure that electrode placement had not changed during scanning.

Data collection. Images were acquired using a 7 tesla spectrometer with 10 gauss/cm gradients using a transverse electromagnetic volume coil. Shimming was optimized to a full-width at half-maximum of ≤40 Hz. fMRI used gradient echo echoplanar (EPI) acquisition using a sinusoidal read gradient, nonlinear sampling, and interpolation to a linear k-space grid. Twenty-three 1-mm-thick slices were acquired at each time point on a 128 × 128 matrix over a 100 mm field of view (0.693 mm^3 resolution). Echo time was 29 ms, and repetition time was 3 s with an acquisition bandwidth of 250 kHz. For anatomical imaging, we used a proton density weighted turbo spin echo (echo factor 4) acquisition. Stimulation was applied in a block design, alternating 60 s off and on blocks. Each cycle (off-on) comprised 40 scans.

Data analysis. For off-line analysis, we used the Oxford Centre for Functional Magnetic Resonance Imaging of the Brain (FMRIB) Software Library and custom-written routines. Data from the initial stimulus cycle for each run was discarded to ensure a steady state. Assessment for gross motion was made by viewing each slice of the time series in a cine loop. Series with evidence of gross head motion were discarded. After stripping of nonbrain voxels using the FMRIB Brain Extraction Tool, analysis was performed using the FMRIB Expert Analysis Tool. Spatial smoothing was applied with a Gaussian kernel of 2 mm. For statistical analysis, we used the FMRIB Improved Linear Model with local autocorrelation correction. *Z* (Gaussianized T/F) statistic images were thresholded using clusters determined by $Z > 3.2$ and a cluster significance threshold of $p = 0.005$ (Woolrich et al., 2001). Mean signal intensity for active clusters was determined at each time point and plotted for the time series. Functional (EPI) images were registered to the anatomic images using a custom-written registration algorithm. Registration parameters were applied to activation maps, which are displayed superimposed on the anatomic images. Other than the statistical criteria applied to the whole brain volume as above, no additional editing or masking of the activation maps was performed.

Anesthesia. fMRI was conducted under anesthesia. Ketamine and xylazine IM were given for brief sedation with atropine to control secretions. Animals were intubated but breathed spontaneously. Isoflurane (0.5–0.8%), N_2O (30–40%), and oxygen (23%) were administered. Heart rate, oxygen saturation, respiratory rate, end-tidal CO_2, blood pressure, and temperature were monitored. fMRI did not commence until at least 2 h after administration of ketamine.

Electrophysiology

Subjects. Three monkeys of the same size and age as those in the fMRI sessions were surgically prepared for awake electrophysiological recording using standard methods (Schroeder et al., 1998) under deep Isoflurane (1–2%) anesthesia. A cranial pedestal incorporating guide tubes for electrode access to the brain and a post to allow painless restraint of the head during electrophysiological recording was implanted.

Stimuli. The stimulation protocol was identical to that used for fMRI, but during recording, animals were maintained in an alert state. The essential features of the laminar response profile in primary somatosensory cortex are the same whether the monkey is awake (Peterson et al., 1995) or anesthetized (Schroeder et al., 1995, 1997). However, conducting electrophysiological experiments in the awake state allows better resolution of subtle physiological effects. Although we judged this to be the optimal way to approach electrophysiological analysis of ipsilateral hand input to area 3b, it should be recognized that the mismatch of the recording conditions limits the ability of the electrophysiology to provide strict interpretation of the fMRI findings. Monkeys were accustomed to a primate chair and head restraint and habituated to the stimulus but were not required to attend to or discriminate stimuli.

Data collection. Our purpose was analysis of the laminar distribution of synaptic activity as well as action potentials. This entailed first recording electrical signals simultaneously from all of the channels of a linear array multielectrode (Barna et al., 1981) (Neurotrack, Budapest, Hungary) positioned within a cortical area with the array running orthogonal to the local lamination pattern. The electrode is shown in a schematic form in Figure 3. Because the electrode array has 14 channels spaced at 150 μm, it can effectively bracket the activity pattern in a cortical region penetrated at an appropriate angle. After an initial preamplification of 10× at the electrode headstage, signals from each electrode channel were amplified 1000× with a bandpass of 1 Hz to 3 kHz and processed separately to extract field potentials and action potentials. Field potentials were obtained by digitizing the raw amplifier outputs and averaging over 50 stimulus presentations. MUA was obtained from the signal at each contact by high-pass filtering the amplifier output at 500 Hz to isolate action potential frequency activity, full-wave rectifying the high-frequency activity, integrating the activity down to 1 kHz, and then digitizing the signal at 2 kHz and averaging the single sweep responses ($n = 50$). This yields an estimate of the envelope firing pattern in local neurons (Legatt et al., 1980). Upward deflection represents an increase in activity, and downward deflection represents activity decrease relative to the prestimulus baseline. The CSD profile was calculated from the field potential profile using a three-point formula for estimation of the second spatial derivative of voltage, which is an index of the transmembrane current flow distribution in the local neuronal ensemble (Nicholson and Freeman, 1975; Schroeder et al., 1995). Transmembrane current flow is the first-order response to synaptic input, which directly generates the extracellular field potential distribution, as well as intracellular IPSPs and EPSPs, the balance of which determine action potential rates (Schroeder et al., 1998).

Statistical analysis. Determination of a statistically significant response was made by comparing the activity present in the baseline CSD and MUA with poststimulus activity using a two-tailed *t* test, with a criterion of $p < 0.05$. For each channel, poststimulus onset latency was determined to be the first of eight consecutive time points with an associated amplitude value of at least three SDs above the mean of the baseline activity. The onset latency for the supragranular, granular, and infragranular laminas was then specified as the earliest onset within the recording channels located in that laminar grouping.

Electrode array positioning and laminar profile analysis. Data for this study were collected during acute penetrations of the hand representation in area 3b. Based on presurgical MRI, the recording electrode was stereotaxically introduced to penetrate frontal cortex and traverse the posterior bank of the central sulcus, entering area 3b perpendicular to its pial surface. Using the stimulus-evoked response, the electrode depth was adjusted so that the array of electrode contacts bracketed the layers of area 3b. A previous report provides detailed description and illustration of this method of functional positioning of a multielectrode array for use in the visual system (Schroeder et al., 1998). The principle is the same in auditory cortices (Schroeder et al., 2001; Fu et al., 2004; Lakatos et al., 2005a,b) and somatosensory cortices (Schroeder et al., 1995, 1997). The method is based on the fact that the electrode array covers ~2 mm linear distance. When advanced slowly through the brain, the electrode array easily detects nonlinear changes (perturbations) in the local field potential gradient. These correspond to regions of active neuronal transmembrane current flow in synapse-rich regions such as the cortex, usually accompanied by action potentials. These regions can be distinguished from intervening white matter zones, because white matter MUA is not accompanied by large, prolonged CSD features (Schroeder et al., 1998) (see Fig. 4). After penetrating to the approximate depth of the region of interest, the position of the array is refined so that it brackets the active cortical region. The practice of making small lesions to help identify locations of interest (Schroeder et al., 1991, 1998) along with previous knowledge of the dimensions of a cortical region and the relative sizes and positions of the laminas allows functional identification of specific cortical laminas. Initial targeting of the electrode penetrations was based on the anatomical location of the activation regions as determined by the functional imaging experiments. Others have reported attempts at colocalization of fMRI and electrophysiology (Disbrow et al., 2000) and noted the inherent difficulties in precisely matching the recording site to the MRI activation site. The goal of our electrophysiological experiment was to define the neural mechanisms of the ipsilateral hand input into area 3b, rather than attempting a point-to-point colocalization of electrophysiological and hemodynamic responses within the region. Each subject first underwent a brief series of mapping penetrations to confirm the localization of the hand representation in area 3b. Both electrical and cutaneous stimuli described in previous studies (Schroeder et al., 1995)

were used during recording from this series of penetrations. Only data from penetrations that entered the hand representation of area 3b were included in this study (i.e., 15 experiments/penetrations). Because relatively few electrode penetrations were required in each subject, two of these monkeys also served as subjects in an unrelated auditory cortical experiment after their participation in this study.

Anatomical reconstruction. The third monkey was a subject in an unrelated anatomical tract tracing experiment after participating in this study. In this case, an anatomical tracer injection was made at one of the physiologically identified area 3b recording sites to confirm histologically that the recording site was within area 3b. After data collection, 0.6 μl of 10% aqueous biotinylated dextran amine (BDA) was injected through a microcannula incorporated into the electrode into the middle layers of the cortex at penetration site Y42. The brain was later perfused with 3 L of 4% buffered paraformaldehyde followed by 1 L each of 10, 20, and 30% buffered sucrose and immersed in 30% sucrose. Coronal blocks were sectioned at 80 μm on a sliding microtome, and adjacent series of every 10th section were processed for cresyl violet, Nissl, parvalbumin immunocytochemistry, and acetylcholinesterase staining (Schroeder et al., 2001). One section containing the BDA injection and associated electrode track through area 3b (Y42) is illustrated in Figure 4*B*.

Results

Figure 1*A* displays a statistical map of the BOLD response to mechanical stimulation of the left hand, registered onto an anatomical image acquired in the same session. Linear clustering of activation deep along the posterior bank of the central sulcus contralateral to the stimulus corresponds to the hand representation in area 3b. Activation was also detected in other somatosensory areas including areas 1, 2, 5, 7, and S2 (data not shown) but is not the subject of this report. The signal time course from the region of activation (Fig. 1*A*) shows correlation of the hemodynamic response with the stimulus cycle and a large magnitude of signal change.

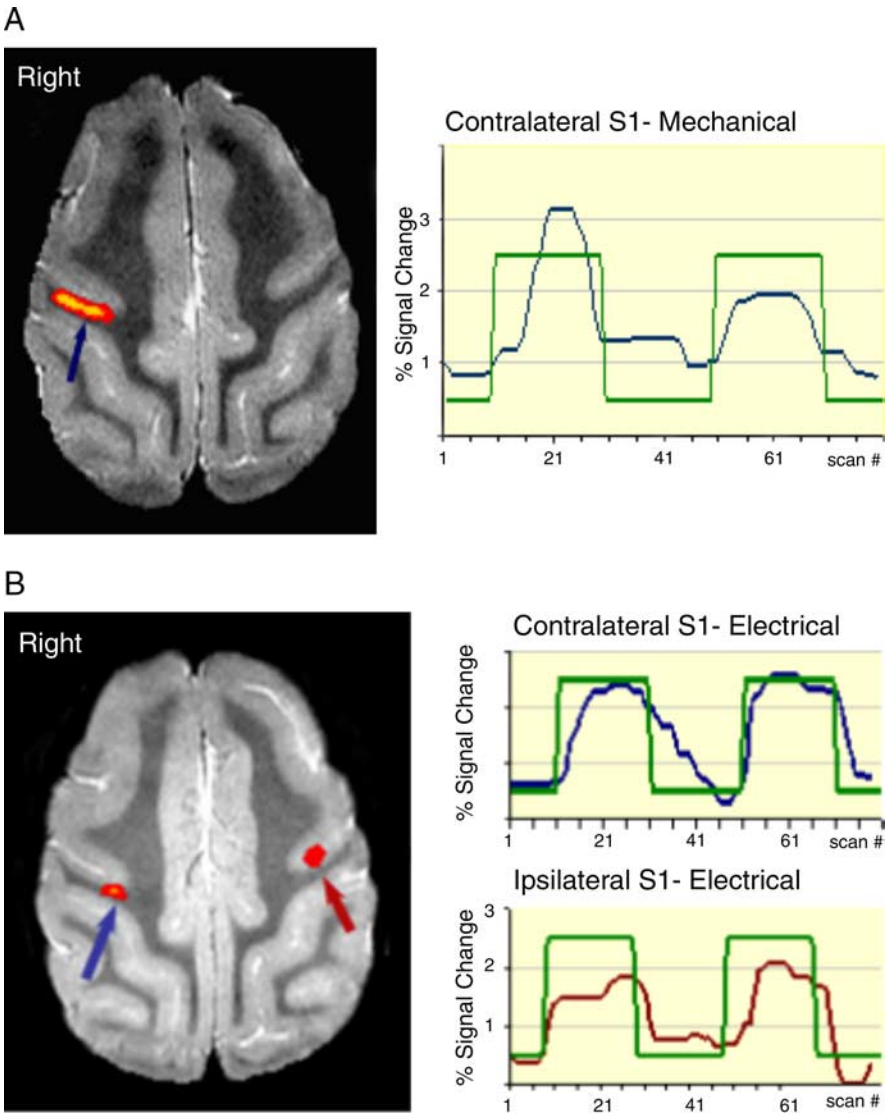

Figure 1. ***A***, fMRI activation map superimposed on an anatomic image shows robust activation (arrow) localized in the depth of the posterior bank of the central sulcus in the hand region of area 3b contralateral to the left-hand stimulus. Signal intensity time course shows correlation with the stimulus paradigm (green boxcar). ***B***, fMRI activation map obtained during left median nerve stimulation in animal 1 superimposed on an anatomic image showing robust activation precisely localized to the hand region of area 3b contralateral to the side of stimulation (blue arrow) as under the cutaneous stimulus (***A***). Additionally, activation is evident in the homologous portion of area 3 ipsilateral to the stimulus (maroon arrow). The signal time course demonstrates greater percentage signal change and improved signal-to-noise contralateral to the stimulus (blue) compared with ipsilateral to the stimulus (maroon).

Median nerve stimulation produced a contralateral fMRI response in area 3b, similar to that produced by mechanical stimulation. However, it also produced a robust ipsilateral area 3b response (Fig. 1*B*), with the same valence of signal intensity change as the contralateral response. This effect was reproduced across subjects (Fig. 2). The contralateral response is predictable based on known anatomy of somatosensory projections, but the large ipsilateral response is paradoxical. To determine the neural correlates of these fMRI responses, we next evaluated electrophysiological responses to contralateral and ipsilateral median nerve stimulation in area 3b.

Figure 3*a* depicts a laminar CSD profile elicited by contralateral median nerve stimulation. This profile is characteristic of feedforward activation in monkey primary somatosensory cortex, whether the subject is anesthetized (Peterson et al., 1995; Schroeder et al., 1995, 2001). The shortest latency response, a current sink (red), occurs in layer 4 and is followed by responses in the extragranular layers. MUA from layer 4 (black tracing superimposed on the CSD profile) shows that the net local response is excitatory. This feedforward laminar activation profile is characteristic of the data set (Fig. 3*b*).

Twelve of 15 area 3b penetrations also detected significant ($p < 0.05$) CSD responses to ipsilateral median nerve stimulation. The ipsilateral response (Fig. 3*c*) contrasts in two main ways with the contralateral response (Fig. 3*a*). First, the ipsilateral CSD profile suggests feedback rather than feedforward response, because initial activity has a longer absolute onset latency (mean, ~23 ms) and begins in extragranular layers, rather than in layer 4. This laminar onset pattern appears characteristic of the data set (Fig. 3*d*). Second, only 4 of 12 recording sites displaying signifi-

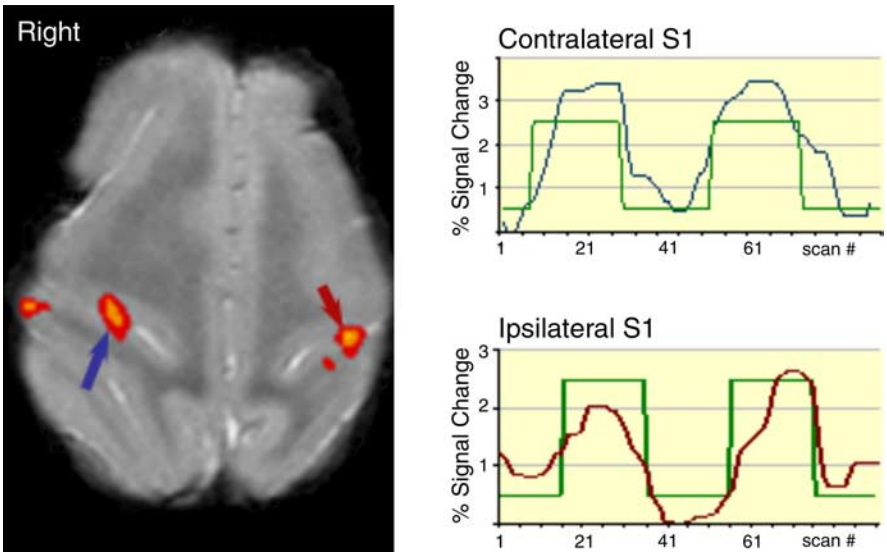

Figure 2. fMRI activation map obtained during left median nerve stimulation of animal 2 and superimposed on an anatomic image demonstrates reproducible activation of the same regions as in animal 1 both contralateral (blue arrow) and ipsilateral to the stimulus (maroon arrow). The corresponding signal time courses are shown.

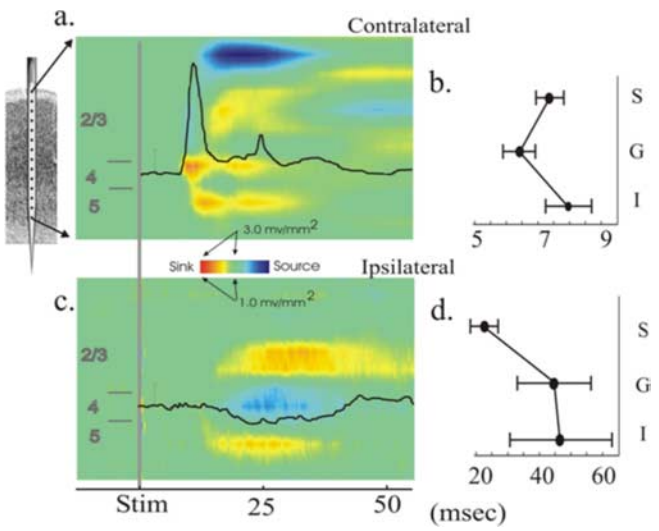

Figure 3. ***a***, A laminar CSD profile elicited in area 3b by electrical stimulation of the contralateral median nerve (schematic of multielectrode at left). MUA from a contact in layer 4 is superimposed on the CSD profile. Current sinks (red) represent net inward transmembrane current flow in the local neuronal population. Current sources (blue) represent net outward current flow. ***b***, Average onset latency and SE as a function of layer (supragranular, granular, and infragranular) of the response to contralateral median nerve stimulation across all 15 electrode penetrations in three subjects. The values comprising the underlying onset latency distributions were derived by taking the earliest point at which the CSD response deviated by >2 SD units from the baseline and remained so for 8 ms. Mean onset latencies were 6.4, 7.3, and 8.0 ms for the granular, supragranular, and infragranular layers, respectively. Latency in layer 4 was significantly earlier ($p < 0.05$) than in the supragranular or infragranular layers. ***c***, The response in the same site to stimulation of the ipsilateral median nerve. This response has a bilaminar pattern typical of feedback input (responses above and below earlier than in lamina 4), with an apparent inhibition (current source) in lamina 4. MUA decrease (black tracing) is associated with the current source that appears in layer 4 in this condition. ***d***, Mean onset latency and SE as a function of layer from the ipsilateral median nerve-evoked response across the 12 of 15 electrode penetrations showing ipsilateral input in the three subjects. Singular values were derived as described for the contralateral condition. Mean onset latencies for the ipsilateral condition were 44.2, 22.8, and 46.7 ms for granular, supragranular, and infragranular layers, respectively. The supragranular mean latency was significantly earlier ($p < 0.05$) than the others.

cant ipsilateral CSD responsiveness displayed associated changes in MUA, but in every case, the observable change was a phasic MUA depression. Three of these cases, one from each of the subjects, are shown in Figure 4*A*. This MUA depression, coupled with the colocated current source, indicates that most of the active local neurons are undergoing hyperpolarization (Schroeder et al., 1998). When there is no preceding net depolarization to generate nonsynaptic refractory processes, such hyperpolarization primarily reflects neuronal inhibition (Schroeder et al., 1998). The localization of the ipsilateral response to area 3b was confirmed histologically (Fig. 4*B*).

Discussion

fMRI

We found clear hemodynamic evidence of ipsilateral input to the hand representation of area 3b. There is no previous study of this type in monkeys. Several previous fMRI studies using electrical stimulation of the median nerve in humans (Spiegel et al., 1999; Backes et al., 2000) reported the expected contralateral response but did not report response in the hand region of area 3b ipsilateral to the stimulus. It is possible that sensitivity to this effect is attributable to imaging at 7 tesla. At a higher magnetic field, the BOLD effect becomes more specific to tissue level, as opposed to large vessel changes (Duong et al., 2000), and the absolute MRI signal increases, allowing higher spatial resolution imaging with acceptable signal-to-noise. The spatial resolution in the present application is 0.693 mm^3, nearly twice that reported at 4.7 T (Logothetis et al., 2001). However, the scale of the effects we report is on the order of several millimeters, within the resolution achievable at lower field strength in humans. This issue requires additional study.

Surprisingly, the spatial extent of activation in response to electrical stimulation (Figs. 2, 3) is smaller than that to mechanical stimulation (Fig. 1). Based on experience with electrophysiology, we expected the powerful median nerve stimulus to elicit a more robust fMRI response than mechanical stimulation. This was not the case, and similar findings in monkeys and humans (Lipton et al., 2004) suggest that it is a real finding. This issue requires additional investigation.

Is the ipsilateral hand response in area 3b unique to electrical stimulation? Preliminary findings from follow-up fMRI studies in monkeys and humans indicate that more natural mechanical stimulation also elicits a bilateral fMRI response in area 3b (Lipton et al., 2004). We are presently investigating this phenomenon using electrophysiology.

Although beyond the scope of the present study, bilateral responses were also detected in other somatosensory areas including areas 1, 2, 5, 7, and S2, most of which are known to have at least some degree of bilateral input. The nature and role of these responses as well as response to simultaneous bilateral stimulation are currently under study.

Electrophysiology

CSD and MUA analysis in area 3b revealed both the ipsilateral and contralateral responses indicated by the fMRI results but also resolved critical differences between them. First, the ipsilateral

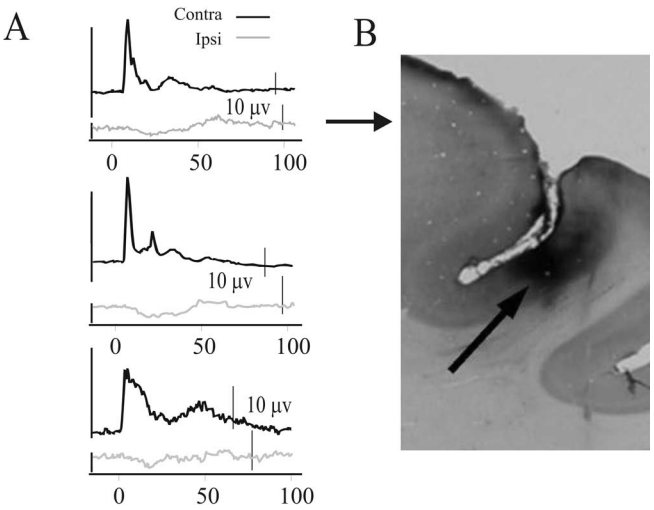

Figure 4. ***A***, Layer 4 MUA recordings from each of the three monkeys in this study, contrasting the contralateral (Contra) median nerve-evoked response (black traces) to the colocated ipsilateral (Ipsi) response (gray traces). ***B***, Histological reconstruction of a BDA deposition in area 3b, made during one of the last penetrations in subject Y, after the recordings in monkey Y shown at the top of ***a***. BDA was microinjected into layer 4, from a microcannula incorporated into the electrode. BDA localization to area 3b (the posterior bank of the central sulcus above area 3a and below area 1) was confirmed by thick parvalbumin staining of lower layer 3 and layer 4. This helped to verify the location of recording sites within area 3b.

response is significantly delayed relative to the contralateral response. In the grouped data, for example, ipsilateral response latency was 22 ms shorter in lamina 3 than in lamina 4. Several previous event-related potential and magnetoencephalography studies (Schnitzler et al., 1995; Kanno et al., 2003) suggested ipsilateral hand response in some part of S1, with ipsilateral responses later than contralateral responses. Second, the contralateral response has a characteristic feedforward pattern, with initial response in lamina 4 followed by responses in the extragranular laminas, whereas the ipsilateral response begins outside of lamina 4. The timing and laminar profile of the ipsilateral response suggests that it is not triggered by feedforward afferents. With initial activity occurring in the extragranular layers, the response pattern is typical of either a lateral or a feedback profile, according to accepted criteria (Rockland and Pandya, 1979; Felleman and VanEssen, 1991). A lateral/callosal pathway is unlikely based on known connectivity. The hand region of area 3b has few callosal connections (Jones and Hendry, 1980; Killackey et al., 1983; Shanks et al., 1985). Based on all of the available data, we suggest that the ipsilateral hand response is mediated by an input that ascends the contralateral pathway to a higher-order cortical area, crosses in the corpus callosum, and is then fed back to area 3b.

Origin of feedback input

One candidate area is S2/PV. Neurons in S2 and PV often display bilateral hand/arm receptive fields (Krubitzer et al., 1995). Both areas S2 and PV have been shown to have callosal connections with the corresponding areas of the contralateral hemisphere (Jones and Powell, 1969a; Disbrow et al., 2001). Both also have reciprocal connections with the contralateral and ipsilateral areas of S1 (Disbrow et al., 2001), including the hand regions of area 3b (Manzoni et al., 1986). Other candidates for the source(s) of ipsilateral responsiveness in area 3b include areas 5 and 2. Some area 5 neurons have bilateral or ipsilateral distal extremity receptive fields (Sakata et al., 1973) as do some area 2 neurons (Iwamura et al., 1994). Areas 5 and 2 receive ipsilateral hand input from both the S2/PV complex and via callosal connections, denser in area 5 than area 2 (Jones and Hendry, 1980), and have extensive reciprocal connections to ipsilateral area 3b (Jones and Powell, 1969b; Kaas, 1993).

Feedback-mediated inhibition

At least as striking as the ipsilateral response in the hand region of area 3b is the nature of this response. The ipsilateral hand response in area 3b appears to reflect net local inhibition. Intriguingly, a previous report of ipsilateral "modulation" of the area 3b hand representation concluded that the main effect was inhibition (Calford and Tweedale, 1990). Given that long-range projections are generally excitatory, how is the inhibition triggered? Excluding a direct, long-range inhibitory input, the simplest possible circuit for this effect would be a descending (feedback) input that drives a local inhibitory interneuron, causing hyperpolarization (inhibition) of one or more local neurons. Although feedback afferents do appear to target inhibitory neurons in neocortex in ~10% of cases (Gonchar and Burkhalter, 1999), the dynamics of feedback interactions tend to favor excitation over inhibition (Shao and Burkhalter, 1996). At the macroscopic scale of the CSD and MUA measurements used in the present study, we cannot definitively distinguish the contribution of local excitatory (glutamatergic) from that of inhibitory (GABAergic) neurons. However, the fact that local excitatory neurons are more numerous and larger than inhibitory neurons in most cortical areas argues that both our electrophysiological and hemodynamic analyses may be biased toward processes occurring in excitatory neurons. Empirically, this seems to be the case; we observed depression of MUA associated with a current source (Fig. 3*b*). This is evidence of net local inhibition driven by the ipsilateral input that is without accompanying evidence of an excitatory response in the local GABAergic neurons that presumably drive the inhibition.

Combining fMRI, CSD, and MUA

Our results underscore the promise of additional experiments using this approach. The neural processes underlying fMRI signals are indexed better by LFPs than by action potentials (Logothetis et al., 2001). CSD, the second derivative of the LFP, indexes transmembrane current flow, which is the first-order response to synaptic activation. The CSD measure is sensitive to the input whether or not it causes local neurons to cross the action potential threshold (Schroeder et al., 1998). Additionally, combined CSD and MUA analysis allows us to identify net underlying neuronal processes and to localize them to specific cortical laminas and cell populations. Our findings, based on this combination of techniques, outline a subtle effect in which net inhibition appears to be associated with a positive BOLD signal, a possibility discussed recently (Lauritzen and Gold, 2003). Although in the present case fMRI apparently does not distinguish between net excitation and net inhibition in the local neuronal ensemble, it is clear that with the appropriate integration of techniques the nature of the underlying neuronal response can be resolved.

References

Backes WH, Mess WH, van Kranen-Mastenbroek V, Reulen JP (2000) Somotosensory cortex responses to median nerve stimulation: fMRI effects of current amplitude and selective attention. Clin Neurophysiol 111:1738–1744.

Barna JS, Arezzo JC, Vaughan Jr HG (1981) A new multielectrode array for the simultaneous recording of field potentials and unit activity. Electroencephalogr Clin Neurophysiol 52:494–496.

Calford MB, Tweedale R (1990) Interhemispheric transfer of plasticity in the cerebral cortex. Science 249:805–807.

Conti F, Fabri M, Manzoni T (1986) Bilateral receptive fields and callosal connectivity of the body midline representation in the first somotosensory area of primates. Somatosens Res 3:273–289.

Disbrow E, Roberts T, Poeppel D, Krubitzer L (2001) Evidence for interhemispheric processing of inputs from the hands in human S2 and PV. J Neurophysiol 85:2236–2244.

Disbrow EA, Slutsky DA, Roberts TP, Krubitzer LA (2000) Functional MRI at 1.5 tesla: a comparison of the blood oxygenation level-dependent signal and electrophysiology. Proc Natl Acad Sci USA 97:9718–9723.

Disbrow EA, Hinkley LB, Roberts TP (2003) Ipsilateral representation of oral structures in human anterior parietal somatosensory cortex and integration of inputs across the midline. J Comp Neurol 467:487–495.

Dreyer DA, Loe PR, Metz CB, Whitsel BL (1975) Representation of head and face in postcentral gyrus of the macaque. J Neurophysiol 38:714–733.

Duong TQ, Silva AC, Lee SP, Kim SG (2000) Functional MRI of calcium-dependent synaptic activity: cross correlation with CBF and BOLD measurements. Magn Reson Med 43:383–392.

Felleman DJ, VanEssen DC (1991) Distributed hierarchical processing in the primate cerebral cortex. Cereb Cortex 1:1–47.

Freeman JA, Stone J (1969) A technique for current source density analysis of field potentials and its application to the frog cerebellum. In: Neurobiology of cerebellar evolution and development (Llinas R, ed), pp 421–430. Chicago: American Medical Association.

Fu KM, Shah AS, O'Connell MN, McGinnis T, Eckholdt H, Lakatos P, Smiley J, Schroeder CE (2004) Timing and laminar profile of eye-position effects on auditory responses in primate auditory cortex. J Neurophysiol 92:3522–3531.

Gonchar Y, Burkhalter A (1999) Differential subcellular localization of forward and feedback interareal inputs to parvalbumin expressing GABAergic neurons in rat visual cortex. J Comp Neurol 406:346–360.

Iwamura Y (1998) Hierarchical somatosensory processing. Curr Opin Neurobiol 8:522–528.

Iwamura Y, Iriki A, Tanaka M (1994) Bilateral hand representation in the postcentral somatosensory cortex. Nature 369:554–556.

Jain N, Qi HX, Catania KC, Kaas JH (2001) Anatomic correlates of the face and oral cavity representations in the somatosensory cortical area 3b of monkeys. J Comp Neurol 429:455–468.

Jones EG, Hendry SH (1980) Distribution of callosal fibers around the hand representations in monkey somatic sensory cortex. Neurosci Lett 19:167–172.

Jones EG, Powell TP (1969a) Connexions of the somatic sensory cortex of the rhesus monkey. I. Ipsilateral cortical connexions. Brain 92:477–502.

Jones EG, Powell TP (1969b) Connexions of the somatic sensory cortex of the rhesus monkey. II. Contralateral cortical connexions. Brain 92:717–730.

Kaas JH (1993) The functional organization of somatosensory cortex in primates. Ann Anat 175:509–518.

Kanno A, Nakasato N, Hatanaka K, Yoshimoto T (2003) Ipsilateral area 3b responses to median nerve somatosensory stimulation. NeuroImage 18:169–177.

Killackey HP, Gould HJ, III, Cusick CG, Pons TP, Kaas JH (1983) The relation of corpus callosum connections to architectonic fields and body surface maps in sensorimotor cortex of new and old world monkeys. J Comp Neurol 219:384–419.

Krubitzer L, Clarey J, Tweedale R, Elston G, Calford M (1995) A redefinition of somatosensory areas in the lateral sulcus of macaque monkeys. J Neurosci 15:3821–3839.

Lakatos P, Pincze Z, Fu KM, Javitt DC, Karmos G, Schroeder CE (2005a) Timing of pure tone and noise-evoked responses in macaque auditory cortex. NeuroReport 16:933–937.

Lakatos P, Shah AS, Knuth KH, Ulbert I, Karmos G, Schroeder CE (2005b) An oscillatory hierarchy controlling neuronal excitability and stimulus processing in the auditory cortex. J Neurophysiol 94:1904–1911.

Lauritzen M, Gold L (2003) Brain function and neurophysiological correlates of signals used in functional neuroimaging. J Neurosci 23:3972–3980.

Legatt AD, Arezzo J, Vaughan Jr HG (1980) Averaged multiple unit activity as an estimate of phasic changes in local neuronal activity: effects of volume-conducted potentials. J Neurosci Methods 2:203–217.

Lipton ML, Fu K-M, Branch CA, O'Connel N, Gerum S, Schroeder CE (2003) Ipsilateral response in area 3b: demonstration with fMRI and electrophysiology. Soc Neurosci Abstr 29:379.12.

Lipton ML, Branch CA, O'Connel N, Gerum S, Schroeder CE (2004) Bilateral response in primary somatosensory cortex to unilateral hand stimulation. Soc Neurosci Abstr 30:642.23.

Logothetis NK (2003) The underpinnings of the BOLD functional magnetic resonance imaging signal. J Neurosci 23:3963–3971.

Logothetis NK, Pauls J, Augath M, Trinath T, Oeltermann A (2001) Neurophysiological investigation of the basis of the fMRI signal. Nature 412:150–157.

Manger PR, Woods TM, Jones EG (1996) Representation of face and intraoral structures in area 3b of macaque monkey somatosensory cortex. J Comp Neurol 371:513–521.

Manzoni T, Conti F, Fabri M (1986) Callosal projections from area SII to SI in monkeys: anatomical organization and comparison with association projections. J Comp Neurol 252:245–263.

Nicholson C, Freeman JA (1975) Theory of current source density analysis and determination of conductivity tensor for anuran cerebellum. J Neurophysiol 38:356–368.

Peterson NN, Schroeder CE, Arezzo JC (1995) Neural generators of early cortical somatosensory evoked potentials in the awake monkey. Electroencephalogr Clin Neurophysiol 96:248–260.

Rockland KS, Pandya DN (1979) Laminar origins and terminations of cortical connections of the occipital lobe in the rhesus monkey. Brain Res 179:3–20.

Sakata H, Takaoka Y, Kawarasaki A, Shibutani H (1973) Somatosensory properties of neurons in the superior parietal cortex (area 5) of the rhesus monkey. Brain Res 64:85–102.

Schnitzler A, Salmelin R, Salenius S, Jousmaki V, Hari R (1995) Tactile information from the human hand reaches the ipsilateral primary somatosensory cortex. Neurosci Lett 200:25–28.

Schroeder CE, Tenke CE, Givre SJ, Arezzo JC, Vaughan Jr HG (1991) Striate cortical contribution to the surface-recorded pattern-reversal VEP in the alert monkey. Vision Res 31:1143–1157.

Schroeder CE, Seto S, Arezzo JC, Garraghty PE (1995) Electrophysiological evidence for overlapping dominant and latent inputs to somatosensory cortex in squirrel monkeys. J Neurophysiol 74:722–732.

Schroeder CE, Javitt DC, Steinschneider M, Mehta AD, Givre SJ, Vaughan Jr HG, Arezzo JC (1997) *N*-methyl-D-aspartate enhancement of phasic responses in primate neocortex. Exp Brain Res 114:271–278.

Schroeder CE, Mehta AD, Givre SJ (1998) A spatiotemporal profile of visual system activation revealed by current source density analysis in the awake macaque. Cereb Cortex 8:575–592.

Schroeder CE, Lindsley RW, Specht C, Marcovici A, Smiley JF, Javitt DC (2001) Somatosensory input to auditory association cortex in the macaque monkey. J Neurophysiol 85:1322–1327.

Shanks MF, Pearson RC, Powell TP (1985) The callosal connexions of the primary somatic sensory cortex in the monkey. Brain Res 356:43–65.

Shao Z, Burkhalter A (1996) Different balance of excitation and inhibition in forward and feedback circuits of rat visual cortex. J Neurosci 16:7353–7365.

Shin HC, Won CK, Jung SC, Oh S, Park S, Sohn JH (1997) Interhemispheric modulation of sensory transmission in the primary somatosensory cortex of rats. Neurosci Lett 230:137–139.

Spiegel J, Tintera J, Gawehn J, Stoeter P, Treede RD (1999) Functional MRI of human primary somatosensory and motor cortex during median nerve stimulation. Clin Neurophysiol 110:47–52.

Towe AL, Patton H, Kennedy T (1964) Response properties of neurons in the pericruciate cortex of the cat following electrical stimulation of the appendages. Exp Neurol 10:325–344.

Whitsel BL, Petrucelli LM, Werner G (1969) Symmetry and connectivity in the map of the body surface in somatosensory area II of primates. J Neurophysiol 32:170–183.

Woolrich MW, Ripley BD, Brady M, Smith SM (2001) Temporal autocorrelation in univariate linear modeling of FMRI data. NeuroImage 14:1370–1386.